Polymer Degradation and Stability 241 (2025) 111570

Contents lists available at ScienceDirect

Polymer Degradation and Stability

journal homepage: www.journals.elsevier.com/polymer-degradation-and-stability

Synthesis of poly(lactic acid) multiblock copolymers with improved properties using 3-hydroxybutyrate diol

Konosuke Yoshida [a], Yu-I Hsu [a,*], Masayuki Sugimoto [b], Hiroshi Uyama [a,*]

[a] Department of Applied Chemistry, Graduate School of Engineering, The University of Osaka, 2-1 Yamadaoka, Suita, Osaka 565-0871, Japan
[b] Advanced Technology Institute, Osaka Gas Co. Ltd., 6-19-9 Konohana-ku, Osaka-city, Osaka 554-0051, Japan

ARTICLE INFO

Keywords:
Poly(lactic acid) (PLA)
(*R*)-3-Hydroxybutyrate (3HB) diol
Copolymer
Biodegradable polymer
Enzymatic degradation
Structure-property relationship

ABSTRACT

The increasing accumulation of persistent plastic waste in terrestrial and marine environments has heightened the demand for high-performance, biodegradable alternatives. Poly(lactic acid) (PLA) is a widely used renewable polyester, yet its intrinsic brittleness and limited degradability under ambient conditions continue to impede broader application. In this work, a fully synthetic strategy was developed to address these limitations through the design of (*R*)-3-hydroxybutyrate (3HB)-Poly(lactic acid) (PLA) multiblock copolymers incorporating structurally tailored 3HB diols. Structurally distinct 3HB diols were synthesized via nucleophilic substitution between chemically derived 3HB and either a linear dihalide or a cyclic ditosylated compound, yielding diols in which two 3HB units are connected by a linear or cyclic linker. These diols were subsequently copolymerized with *L*-lactide via ring-opening polymerization, followed by chain extension using hexamethylene diisocyanate (HDI) to obtain alternating multiblock copolymers. The resulting materials exhibited significantly enhanced mechanical properties, with linear 3HB diols notably improving toughness and elongation at break. Differential scanning calorimetry revealed that 3HB incorporation reduced the glass transition temperature, while variation in PLA segment length modulated crystallinity. Enzymatic degradation assays showed substantially faster degradation rates compared to neat PLA, confirming improved biodegradability. These results demonstrate that incorporating chemically modified 3HB diols into PLA enables concurrent enhancement of mechanical performance and environmental biodegradability. Furthermore, the tunability of material properties through control of 3HB architecture and PLA segment length highlights the versatility of this copolymer design strategy for developing sustainable polymer systems.

1. Introduction

Plastics have become indispensable in modern society due to their exceptional durability, processability, and low production costs. However, their persistent accumulation in the environment has become a pressing global issue, with approximately 11 million metric tons of plastic waste entering marine ecosystems annually [1,2]. Because of their resistance to natural degradation [3], conventional petroleum-based plastics persist in landfills and aquatic environments, posing long-term risks to both ecological and human health [4–6]. This concern has spurred increasing interest in the development of sustainable materials capable of degrading under environmental conditions without producing harmful residues. Biodegradable polymers offer a promising alternative, as they undergo hydrolytic or enzymatic degradation into non-toxic byproducts, thereby reducing the environmental footprint of traditional plastics [7,8]. In support of this transition, policy initiatives such as the European Union's Single-Use Plastics Directive and Japan's Biomass Plastic Strategy have actively promoted the adoption of biodegradable materials [9–11]. However, to serve as viable substitutes in mainstream applications, these materials must also demonstrate adequate mechanical and thermal performance alongside their biodegradability.

Poly(lactic acid) (PLA), a thermoplastic aliphatic polyester derived from renewable resources, is one of the most commercially viable biodegradable polymers. Its high tensile strength and biocompatibility have enabled its use in biomedical devices, packaging, and agricultural films [12]. Nevertheless, PLA suffers from inherent brittleness [13,14], low impact resistance [15–17], and slow degradation under ambient

* Corresponding authors at: Department of Applied Chemistry, Graduate School of Engineering, The University of Osaka, 2-1 Yamadaoka, Suita, Osaka 565-0871, Japan.
E-mail addresses: yuihsu@chem.eng.osaka-u.ac.jp (Y.-I. Hsu), uyama@chem.eng.osaka-u.ac.jp (H. Uyama).

https://doi.org/10.1016/j.polymdegradstab.2025.111570
Received 25 April 2025; Received in revised form 17 July 2025; Accepted 23 July 2025
Available online 23 July 2025

conditions [18,19]. Although industrial composting facilitates PLA degradation, it remains largely stable in natural environments, with minimal mass loss observed even after prolonged exposure to seawater [20,21]. These limitations have prompted efforts to improve both the mechanical and degradation properties of PLA through molecular level modifications.

Various strategies have been explored to overcome these challenges, including blending with flexible polymers, filler reinforcement, and copolymerization. Blending PLA with polycaprolactone (PCL) is a widely studied method to improve toughness, as PCL is a soft, biodegradable polymer with an elongation at break of approximately 600 %, attributed to its low glass transition temperature (T_g) [22]. For example, 80/20 PLA/PCL blends exhibit enhanced elongation at break due to the ductile nature of PCL [23]. However, their distinct polarities and molecular structures lead to immiscibility and phase separation, which limits interfacial stress transfer and overall mechanical reinforcement [24,25]. Similar compatibility issues are observed in blends of PLA with poly(butylene adipate-*co*-terephthalate) (PBAT), where poor interfacial adhesion compromises toughness and durability [26]. To overcome these shortcomings, the use of compatibilizers [27,28] or reactive extrusion techniques [29] is often required to enhance interfacial bonding and stabilize phase morphology. Inorganic fillers such as glass fibers are commonly incorporated into PLA to enhance mechanical strength and thermal stability. Composites containing approximately 30 wt % glass fibers have demonstrated significant improvements in stiffness, tensile strength, and heat deflection temperature compared to neat PLA [30]. However, challenges such as moisture sensitivity [31] and poor interfacial adhesion between layers [32] must be addressed to fully exploit the benefits of glass fiber reinforcement. In contrast, organic fillers such as cellulose nanomaterials are attractive due to their low cost, renewable origin, low density, and high intrinsic stiffness. Despite these advantages, the hydrophilic nature of cellulose often leads to poor dispersion and weak interfacial bonding within the hydrophobic PLA matrix, which can compromise mechanical performance [33]. While filler addition is a relatively simple strategy for property enhancement, the choice and loading level of fillers must be carefully optimized [30]. Excessive filler content can reduce mechanical properties and, in the case of non-degradable or inert fillers, may hinder overall biodegradability.

Among these approaches, copolymerization stands out as the most versatile and effective method for property enhancement. By modifying the polymer backbone at the molecular level, copolymerization enables simultaneous improvements in flexibility, toughness, and biodegradability while maintaining material homogeneity. For example, Takagi et al. synthesized PLA-PCL-PLA triblock copolymers via ring-opening polymerization (ROP) of *L*-lactide using PCL-diol as an initiator. The resulting copolymers exhibited tunable mechanical properties depending on PLA segment length, showing increased elongation at break, improved toughness, and significantly accelerated degradation under composting conditions [34]. Similarly, He, et al. developed sequence-controlled poly(ethylene glycol) (PEG)-PLA copolymers with enhanced flexibility and adjustable degradation rates in both enzymatic and marine environments. The incorporation of hydrophilic PEG units increased water uptake and facilitated ester bond hydrolysis by enhancing interactions with water molecules, thereby promoting nucleophilic attack on the backbone [35]. While effective, the copolymerization approach often results in relatively low molecular weights, which can adversely affect mechanical performance [36]. To address this limitation, chain extension using hexamethylene diisocyanate (HDI) was employed, particularly in the development of PLA-based thermoplastic polyurethanes (TPUs), to enhance molecular weight and modulate mechanical properties. This approach enables the formation of multiblock architectures without compromising biodegradability or structural compatibility. In this context, the choice of comonomers is critical in this approach, especially those that are both biodegradable and structurally compatible with PLA.

(*R*)-3-Hydroxybutyrate (3HB), the monomeric unit of poly(3-hydroxybutyrate) (PHB), is a particularly promising candidate due to its excellent biodegradability and structural compatibility with PLA. PHB has demonstrated relatively rapid degradation in marine environments, with substantial mass loss observed within a short period [37]. However, its high crystallinity contributes to brittleness, limiting its use in applications requiring flexibility [38]. To overcome this, structural modification of 3HB has been explored as a means to reduce crystallinity and improve mechanical properties. For example, incorporation of 3-hydroxyhexanoate (3HHx) yields the copolymer poly(3-hydroxybutyrate-*co*-3-hydroxyhexanoate) [P(3HB-*co*-3HHx)], which exhibits elastomeric behavior characterized by reduced crystallinity, high elasticity, and significantly increased elongation at break [39]. Likewise, copolymerization with 4-hydroxybutyrate (4HB) produces poly(3-hydroxybutyrate-*co*-4-hydroxybutyrate) [P(3HB-*co*-4HB)], in which the flexible 4HB segments disrupt crystalline packing, leading to a marked reduction in crystallinity and crystallization rate while also mitigating the inherent brittleness of PHB [40]. These findings underscore the effectiveness of molecular tailoring in modulating the mechanical and degradation properties of PHB-based materials and highlight 3HB structural modification as a viable strategy for enhancing flexibility and biodegradability in bio-based polyesters.

Copolymerization of PLA with 3HB has been widely studied to enhance material properties. Abe et al. synthesized random copolymers of 3HB and (*S,S*)-lactide via ROP, showing that T_g, crystallinity, and enzymatic degradability were strongly dependent on lactide content [41]. Yamada et al. demonstrated microbial production of optically pure random P(LA-*co*-3HB) with enriched lactate composition, enabling biosynthetic control of copolymer structure [42]. For enhanced mechanical performance, Hiki et al. prepared ABA-type triblock copolymers using racemic PHB as the soft segment and PLA as the hard segment, achieving thermoplastic elastomer properties tunable by the lactide/PHB feed ratio [43]. Wu et al. expanded on this by synthesizing PHB-PLA-PCL triblock copolymers with improved flexibility and biocompatibility [44]. Tabata and Abe examined the effects of copolymer composition and sequential structures on the thermal properties of 3HB/lactate copolymers, revealing that T_g depended on composition, melting temperature (T_m) on sequential length, and crystallinity on both factors [45]. However, despite the recognized influence of 3HB structural modification on polymer properties, a thorough investigation into the effect of 3HB segment topology at a fixed segment length and a controlled preparation of structurally defined 3HB segments within 3HB/PLA copolymers has not yet been conducted. Furthermore, while the impact of extended 3HB segments has been explored, the specific contribution of the 3HB unit itself to copolymer properties has received limited attention.

Building on this concept, the present study investigates a fully synthetic approach for tailoring PLA-based materials through the incorporation of 3HB diols with controlled molecular architecture. Linear and cyclic 3HB diols were synthesized via nucleophilic substitution between chemically derived 3HB and either a linear dihalide or a cyclic ditosylated compound, yielding diols in which two 3HB units are connected by a linear or cyclic linker. These diols were copolymerized with PLA via ROP of *L*-lactide, followed by chain extension using HDI, to produce high-molecular-weight 3HB-PLA multiblock copolymers with alternating segment structures (Fig. 1). This synthetic design enables systematic investigation of how variations in 3HB molecular structure and PLA segment length influence thermal transitions, mechanical behavior, and enzymatic degradability. By introducing structural control at the diol level, a parameter rarely examined in PLA copolymer systems, this study establishes a modular and tunable framework for addressing the performance limitations of PLA. The resulting approach contributes to the molecular design of biodegradable polyesters and offers a versatile strategy for developing high-performance materials tailored for sustainable packaging, biomedical, and environmental applications.

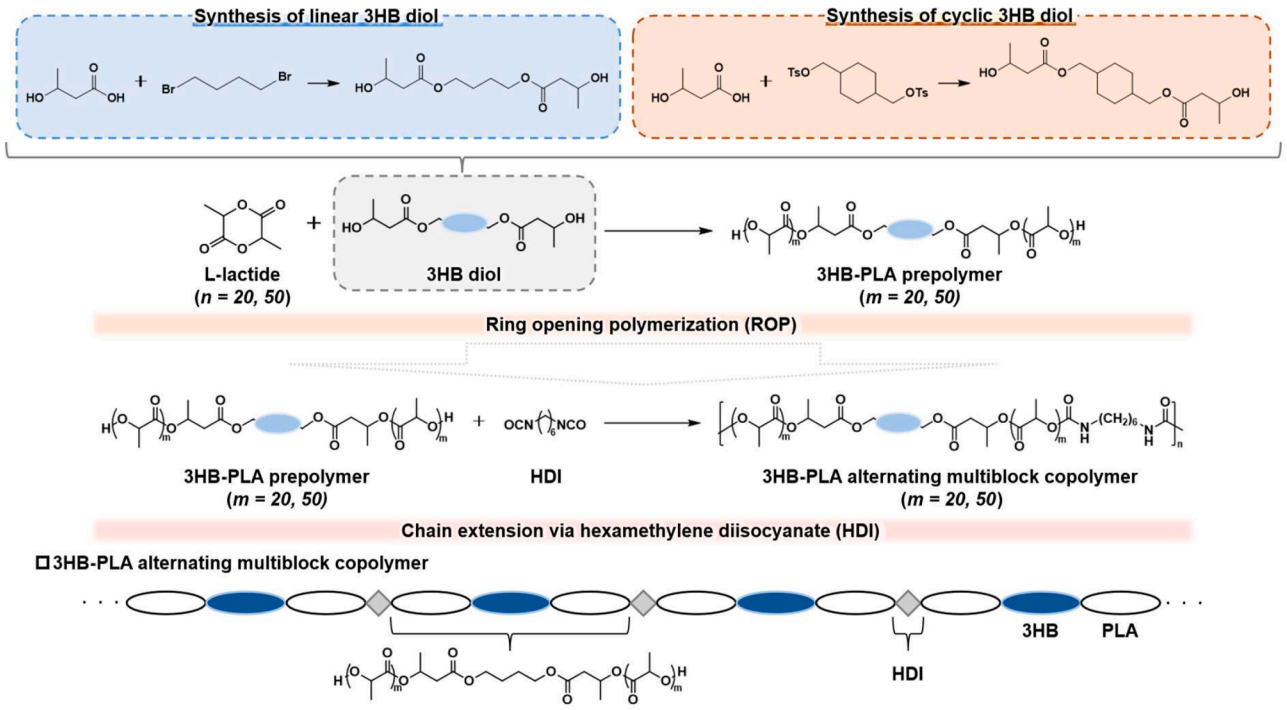

Fig. 1. Schematic of 3HB-PLA alternating multiblock copolymer synthesis via ROP and chain extension.

2. Materials and methods

2.1. Materials

(*R*)-3-hydroxybutyric acid (3HB) was provided by Osaka Gas Co., Ltd. (Osaka, Japan). The following reagents and solvents were purchased from Wako Pure Chemical Industries (Osaka, Japan): 1,4-cyclohexanedimethanol (mixture of cis- and trans-) (CHDM, 1st grade), *N, N, N', N'*-tetramethyl-1,6-hexanediamine (special grade), triethylamine (special grade), acetonitrile (GR grade), chloroform ($CHCl_3$, GR grade), methanol (CH_3OH, GR grade), potassium carbonate (K_2CO_3, GR grade), hexane (GR grade), sodium chloride (GR grade), magnesium sulfate (anhydrous, special grade), sodium carbonate (Na_2CO_3, GR grade), tin (II) 2-ethylhexanoate ($Sn(Oct)_2$, >95 %), proteinase K (recombinant), and sea sand (425 - 850 μm, 20 - 35 mesh, practical grade). *p*-toluenesulfonyl chloride (>99 %), *N, N'*-dimethylethylenediamine (>97 %), 1,4-dibromobutane (>98 %), 1,4-butanediol (>99 %), *L*-lactide (>98 %), and hexamethylene diisocyanate (HDI, >98 %) were purchased from Tokyo Chemical Industry Co., Ltd. (Tokyo, Japan). *N, N*-Dimethylformamide (DMF, GR grade) and ethyl acetate (1st grade) were obtained from Nacalai Tesque Inc. (Kyoto, Japan). Poly(*L*-lactide) (PLA, M_n = 59,000, <0.5 % water) and celite 503 (CP) were purchased from Sigma-Aldrich Japan LLC (Tokyo, Japan). A pH 8.5 buffer solution of 1 mol L^{-1} Tris hydrochloride (Tris-HCl) was purchased from Nippon Gene Co., Ltd. (Tokyo, Japan). All reagents were used as received unless otherwise stated. PLA was first dissolved in $CHCl_3$ and then reprecipitated in CH_3OH to remove impurities and ensure consistent preparation conditions with the copolymers. Deionized (DI) water purified using a Mili-Q system (Millipore Inc., Milford, MA, USA) was used for all experiments.

2.2. Synthesis of 3HB-PLA multiblock copolymer

2.2.1. Synthesis of butane-3HB diol

3HB (8.75 g, 84.05 mmol) and 1,4-dibromobutane (8.24 g, 38.17 mmol) were dissolved in 40 mL of DMF and stirred at room temperature under a nitrogen atmosphere. K_2CO_3 (11.62 g, 84.07 mmol) was then added, resulting in the evolution of carbon dioxide. After approximately 30 min, the reaction mixture gelled. An additional 40 mL of DMF was added to facilitate stirring, and the reaction was heated to 80 °C and maintained under these conditions with continuous stirring for 18 h, yielding a white slurry. The reaction mixture was filtered through celite pad, and the solvent was removed under reduced pressure (60 °C, 0.2 kPa), affording a pale-yellow oil. The crude product was purified by column chromatography using hexane/ethyl acetate (1:11, v/v) as the eluent, yielding 1,4-butanediol bis(3-hydroxybutanoate) (butane-3HB diol) as a transparent oil (6.31 g, 63.1 % yield).

2.2.2. Synthesis of cyclohexane-3HB diol

CHDM (3.51 g, 24.3 mmol), triethylamine (7.39 g, 73.0 mmol), and *N, N', N'*-tetramethyl-1,6-hexanediamine (0.84 g, 4.87 mmol) were dissolved in 100 mL of acetonitrile and cooled in an ice bath under a nitrogen atmosphere. A solution of *p*-toluenesulfonyl chloride (13.92 g, 73.0 mmol) in 100 mL of acetonitrile was added dropwise over 1 hour. The mixture was stirred at 0 °C for 1 hour and then allowed to warm to room temperature, followed by continuous stirring for 24 h. Subsequently, *N, N'*-dimethylethylenediamine (21.8 g, 24.7 mmol) was added, and the mixture was diluted with 100 mL of water. The resulting reaction mixture was filtered, washed thoroughly with 1 L of water, and dried under reduced pressure. The crude product was dissolved in 200 mL of $CHCl_3$ and CH_3OH (1:1, v/v) with gentle heating. Upon cooling, the precipitate was collected via filtration and dried under reduced pressure yielding CHDM-Ts as a white crystal (4.95 g, 45.1 % yield).

Synthesized CHDM-Ts (9.20 g, 20.3 mmol) and 3HB (4.66 g, 44.8 mmol) were dissolved in 150 mL of DMF and stirred until fully dissolved. K_2CO_3 (6.18 g, 44.8 mmol) was then added, and the reaction mixture was stirred at 50 °C for 48 h. After completion, the mixture was diluted with 500 mL of water and extracted three times with a 3:1 (v/v) mixture of hexane and ethyl acetate (500 mL each). The combined organic layers were washed with 500 mL of brine, dried over anhydrous magnesium sulfate, and concentrated under reduced pressure. The crude product was purified by column chromatography using hexane/ethyl acetate (1:1, v/v) as the eluent, yielding 1,4-cyclohexanedimethanol bis(3-hydroxybutanoate) (cyclohexane-3HB diol) as a transparent oil (2.06

g, 22.4 % yield).

2.2.3. Synthesis of 3HB-PLA alternating multiblock copolymers

The synthesis of 3HB-PLA alternating multiblock copolymers was performed in two steps, ROP of *L*-lactide followed by chain extension with HDI. This stepwise approach was adapted from a previously reported method designed to retain multiblock architecture by minimizing sequence randomization [34]. Two types of synthesized 3HB-diols, butane-3HB diol and cyclohexane-3HB diol, were used as initiator to synthesize butane-3HB-PLA polyurethane (BPPU) and cyclohexane-3HB-PLA polyurethane (CPPU), respectively.

The PLA segment length on each side of the 3HB diol was controlled by adjusting the molar ratio of 3HB diol to *L*-lactide. For PPU-20 (BPPU-20 and CPPU-20), 3HB diol was added at a 1:20 molar ratio with *L*-lactide, while for PPU-50 (BPPU-50 and CPPU-50) was synthesized with a 1:50 molar ratio. Here, the number "20″ and "50" correspond to the average number of lactic acid repeat units on each side of the 3HB diol in multiblock copolymer structure, resulting in four distinct copolymers: BPPU-20, BPPU-50, CPPU-20, and CPPU-50.

In a 100 mL three-neck round-bottom flask, *L*-lactide (10.00 g, 6.94 mmol) was added and vacuum-dried at 60 °C for 1 hour. After drying, the appropriate 3HB diol and $Sn(Oct)_2$ (1 mol % of the hydroxyl end of 3HB diol) were added, and the mixture was further vacuum-dried for another hour. ROP was carried out at 180 °C for 3 h under a nitrogen atmosphere. Upon completion of ROP, HDI (1.5 equivalents relative to the added 3HB diol) was added for the chain extension step, which proceed at 180 °C for 30 min with stirring under a nitrogen atmosphere. The reaction mixture was dissolved in $CHCl_3$, precipitated into an excess volume of CH_3OH under vigorous stirring. The resulting white solid was collected by filtration, washed with CH_3OH, and vacuum-dried at 40 °C to yield the final BPPU and CPPU copolymers with varying PLA segment lengths.

Control multiblock copolymers without 3HB units were synthesized using the same procedure, substituting the 3HB diols with 1,4-butanediol or 1,4-cyclohexanedimethanol as the initiator.

2.2.4. Preparation of 3HB-PLA alternating multiblock copolymer films

Thin films of 3HB-PLA alternating multiblock copolymers and PLA were prepared via solvent casting. The purified polymer samples were dissolved in $CHCl_3$ and cast into a horizontal Teflon mold. The solvent was allowed to evaporate naturally at ambient temperature in a fume hood for three days. The resulting films, with a thickness of approximately 0.2 to 0.3 mm, were subsequently vacuum-dried for 24 h to remove residual solvent and then carefully sealed for further testing. To ensure stabilized physical properties, the films were stored under ambient conditions for at least seven days prior to characterization.

2.3. Characterization and measurements

The molecular structure and chemical composition of 3HB-PLA alternating multiblock copolymers and PLA were confirmed using proton nuclear magnetic resonance (^{1}H NMR) spectroscopy. Spectra were recorded on a JNM-ECS400 spectrometer (400 MHz, JEOL Ltd., Tokyo, Japan) at room temperature, using chloroform-d ($CDCl_3$) as the solvent. The chemical functionalities of the samples were analyzed using attenuated total reflection Fourier transform infrared (ATR-FTIR) spectroscopy. Spectra were recorded on a Nicolet iS20 spectrometer (Thermo Fisher Scientific, MA, USA), scanning 100 times over a wavelength range of 3500–500 cm^{-1}. Molecular weight distributions were determined by gel permeation chromatography (GPC) using a JASCO HLC system (Tokyo, Japan) operated at 40 °C. DMF was used as the eluent at a flow rate of 0.75 mL min^{-1}, with a sample concentration of 10 mg mL^{-1} and an injection volume of 50 μL. The system was calibrated with polystyrene standards (590 to 1.09 × 10^6 Da). The optical transparency of the samples was evaluated using a UV–Vis spectrophotometer (V-750, JASCO, Tokyo, Japan), scanning over a wavelength range of 400–800 nm. Haze properties were assessed with a haze meter (NDH 4000, Nippon Denshoku, Tokyo, Japan). Thermal transition properties, including glass transition temperature (T_g), crystallization temperature (T_c), and melting temperature (T_m), were analyzed using differential scanning calorimetry (DSC200, Hitachi, Tokyo, Japan) under a nitrogen atmosphere at a flow rate of 50 mL min^{-1}. Samples (~8 mg) were heated from 25 to 200 °C at a rate of 10 °C min^{-1}, held for 2 min to remove thermal history, cooled to −30 °C at a rate of 10 °C min^{-1}, and reheated to 200 °C at 10 °C min^{-1}. The crystalline structure of the samples was analyzed using X-ray diffraction (XRD) (Smart-Lab, Rigaku Corporation, Japan) with Cu-Kα radiation (λ = 1.541 Å) at room temperature. The scanning speed was 5° min^{-1}, covering a 2θ range of 5°–60°, with an applied voltage of 45 kV and a current of 200 mA. The degree of crystallinity (X_c) was calculated from the XRD patterns by comparing the area under the crystalline peaks to the total diffraction area (crystalline + amorphous), using the baseline method. Peak fitting and area integration were performed using OriginLab software. Thermal stability and weight loss behavior of the samples were assessed using thermogravimetric analysis (TGA) (STA 200RV, Hitachi, Tokyo, Japan). Measurements were conducted in the temperature range of 30–400 °C at a heating rate of 10 °C min^{-1} under a nitrogen atmosphere with a flow rate of 50 mL min^{-1}. The water contact angle (WCA) of the films was obtained using a basic contact angle meter (DMs-401, Kyowa Interface Science, Saitama, Japan). A 1.0 μL water droplet was placed on the sample surface at room temperature, and the contact angle was measured 10,000 ms after droplet deposition. Each measurement was performed in triplicate, and results were reported as the mean values. The mechanical properties of the films were evaluated using a universal testing machine (Shimadzu AGS-X, Kyoto, Japan) equipped with a 100 N load cell. Tensile tests were performed at a crosshead speed of 10 mm min^{-1} at room temperature. Dumbbell-shaped specimens (2.0 mm × ~0.3 mm, width × thickness) were prepared using a precision cutter, and at least three samples were tested for each formulation. The surface morphology of the films before and after degradation was examined using scanning electron microscopy (SEM, SU3500, Hitachi, Tokyo, Japan) operated at 10 kV. Prior to imaging, the films were sputter-coated with gold using an MSP-1S magnetron sputter (Vacuum Device Inc., Osaka, Japan) to enhance conductivity.

2.4. Enzymatic degradation test

The enzymatic degradation behavior of 3HB-PLA alternating multiblock copolymer films and neat PLA films was evaluated using proteinase K. Uniform film specimens (~5.0 mg, 0.2–0.3 mm thickness) were cut into small pieces and immersed in 5 mL of a 0.05 mol/L Tris-HCl buffer solution (pH 8.5) containing proteinase K at a concentration of 0.4 mg/mL (specific activity: 29 units/mg). The degradation behaviors were performed at 20 °C in a shaking incubator set at 70 rpm. At predetermined time intervals, the samples were removed, thoroughly rinsed with distilled water to stop the enzymatic reaction, and vacuum-dried to a constant weight. The extent of degradation was quantified by calculating weight loss (%) according to the following equation:

$$\textit{Weight loss}\ (\%) = \frac{W_0 - W_t}{W_0} \times 100 \quad (1)$$

where W_0 is the initial dry weight and W_t is the dry weight after degradation.

For comparison, neat PLA films were subjected to identical enzymatic degradation conditions. Morphological changes before and after degradation were observed using SEM.

3. Results and discussion

3.1. Synthesis and characterization of 3HB-PLA multiblock copolymers

Two structurally distinct 3HB diols were synthesized and employed as initiators for the preparation of alternating multiblock copolymers with PLA. These included a linear 1,4-butanediol bis(3-hydroxybutanoate) (butane-3HB diol) and a cyclic 1,4-cyclohexanedimethanol bis(3-hydroxybutanoate) (cyclohexane-3HB diol). Both diols were obtained via nucleophilic substitution between 3HB and either a dihalide or a ditosylated compound under basic conditions, followed by purification through column chromatography. The incorporation of these two topologically distinct diols enabled a systematic investigation of how the structure of the initiator, either linear or cyclic, affects the thermal, structural, and degradation properties of the resulting copolymers. The linear butane-based diol was expected to confer greater segmental flexibility, while the cyclohexane-based diol, due to its conformational rigidity, was anticipated to introduce more constrained and compact domains, potentially affecting crystallization behavior and enzymatic degradation. ^{1}H NMR spectra of the synthesized diols (Fig. S1 and S2) confirmed successful incorporation of both the 3HB moieties and the respective bridging structures. In both cases, the presence of methylene proton signals adjacent to hydroxyl groups at approximately 4.2 ppm in the ^{1}H NMR spectra confirmed the presence of hydroxyl end groups, supporting the suitability of these diols as initiators for subsequent ROP.

3HB-PLA alternating multiblock copolymers were synthesized through a two-step process consisting of ROP of *L*-lactide initiated by 3HB diols, followed by chain extension using HDI. The feed ratio of *L*-lactide to diol was set to either 20 or 50 equivalents to obtain PLA segments with different chain lengths, which also correspond to the number of lactic acid repeat units attached to each side of the 3HB diol. Four copolymers were prepared: BPPU-20 and BPPU-50, derived from the linear butane-3HB diol, and CPPU-20 and CPPU-50, derived from the cyclic cyclohexane-3HB diol.

The chemical structures of the synthesized copolymers were confirmed by ^{1}H NMR spectroscopy. Fig. 2 shows the spectrum of BPPU alongside that of PLA for comparison, while Fig. 3 presents the corresponding spectrum for CPPU. In both cases, distinct signals corresponding to PLA, 3HB, and urethane components were observed, confirming the successful formation of the intended multiblock polyurethane structures. The methyl (CH_3) and methine (CH) protons of the lactic acid repeat units appeared at approximately 1.5 ppm (a) and 4.9–5.2 ppm (b), respectively. A broad resonance at 3.1 ppm (c) was attributed to methylene (CH_2) protons adjacent to the urethane linkage, serving as clear evidence of chain extension by HDI. This assignment was further supported by the appearance of additional CH_2 signals from the HDI spacer at 1.3 ppm (d) and 1.5 ppm (e), which were absent in the spectrum of pure PLA. The 3HB moieties were identified by signals at 1.3 ppm (f) for the CH_3 group, 2.5–2.6 ppm (g) for the CH_2 group next to the carbonyl, and 5.2–5.4 ppm (h) for the CH protons of the 3HB units. In BPPU, the CH_2 protons adjacent to the ester bond (CH_2OCO) from the 3HB unit appeared at 4.1 ppm (i), and the CH_2 protons from the butane segment were observed at 1.7 ppm (j). In CPPU, the corresponding CH_2OCO signal appeared at 3.9 ppm (i), while CH_2 groups from the cyclohexane ring were observed at 1.3 ppm (j), 1.6 (k), and 1.8 ppm (l). The PLA segment lengths, defined as the number of lactic acid repeat units adjacent to the 3HB units, were determined from the integration ratio of PLA and 3HB signals, as described in Eq. (2). These values are summarized in Table 1 and were in close agreement with the theoretical lengths calculated from the *L*-lactide feed ratio, confirming the successful synthesis of copolymers with well-defined PLA segments.

$$\frac{\int^{b} = \text{ lactide units}}{\int^{i} = \text{ 3HB units}} = m \ (\textit{PLA segement length}) \quad (2)$$

The chemical structures of PLA and the 3HB-PLA alternating multiblock copolymers were further characterized by FT-IR spectroscopy (Fig. S3). All samples exhibited characteristic absorption bands corresponding to PLA, while the copolymers additionally showed a distinct band at 1530 cm^{-1}, attributed to N-H bending ($\delta_{N\text{-}H}$) from urethane linkages. Notably, the intensity of this urethane-related band was higher in BPPU-20 and CPPU-20 than in their longer-chain counterparts, reflecting the higher relative content of urethane groups resulting from

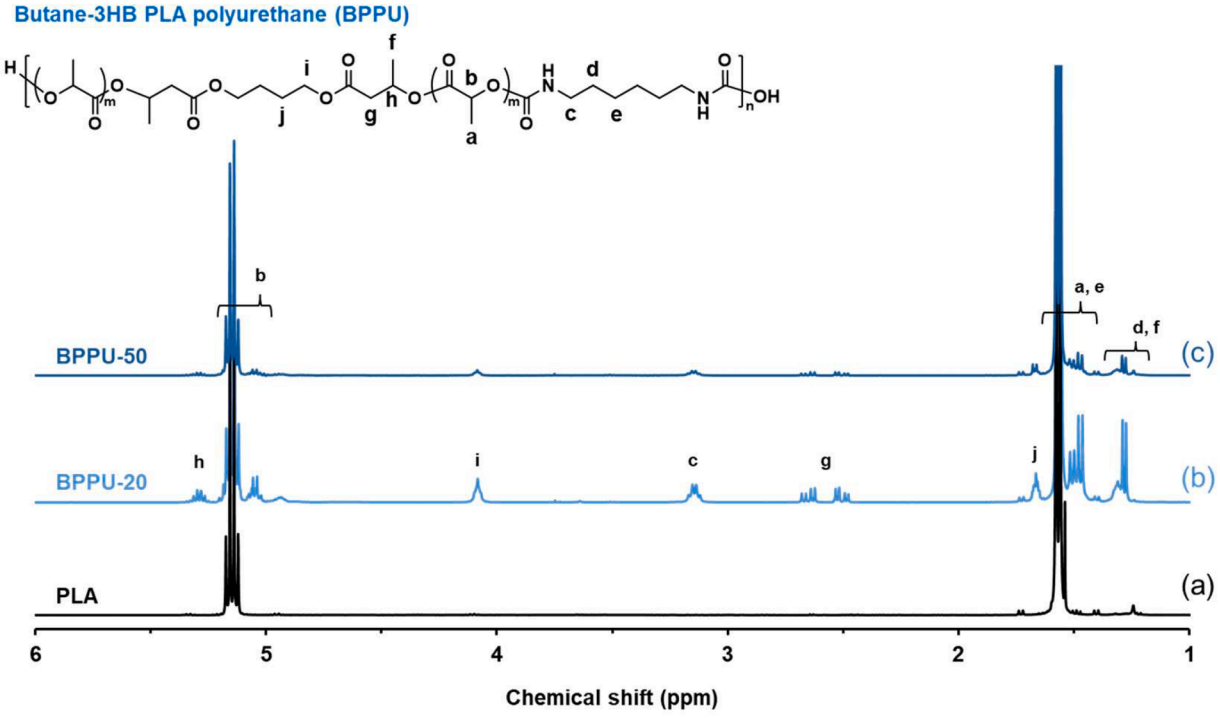

Fig. 2. ^{1}H NMR spectra of (a) PLA, (b) BPPU-20, and (c) BPPU-50 copolymers.

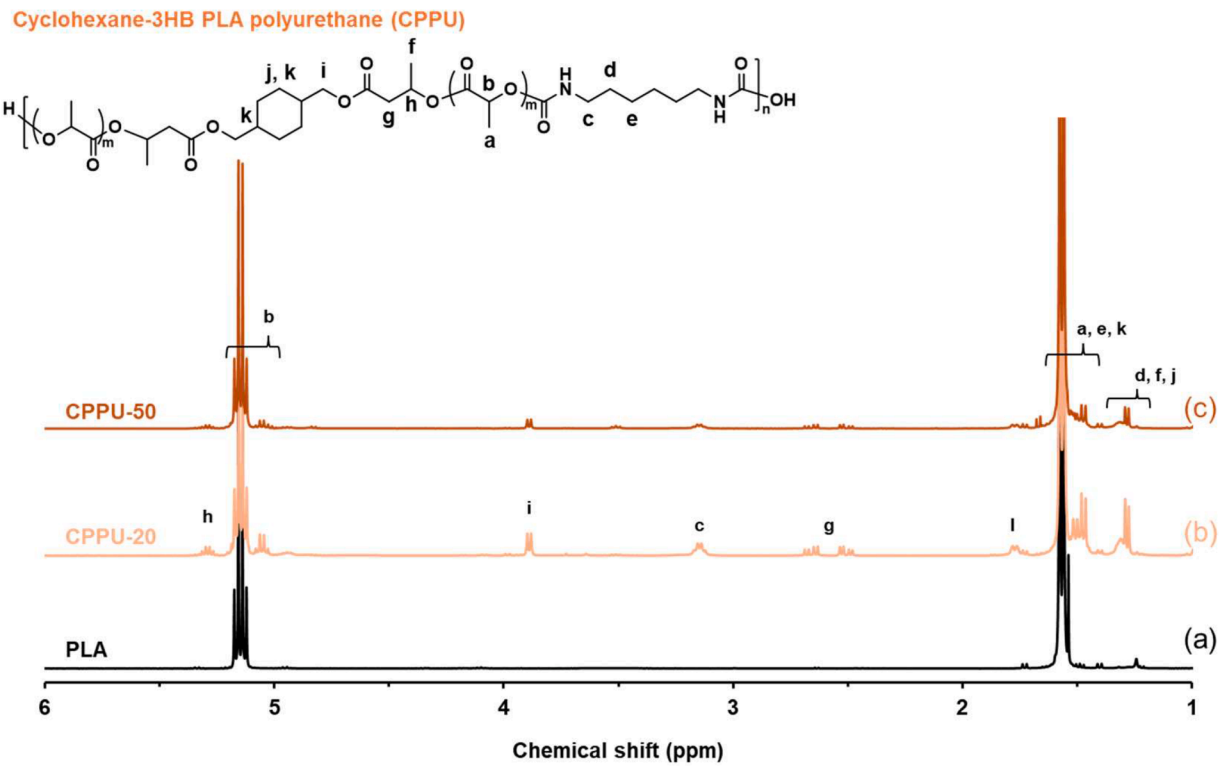

Fig. 3. ^{1}H NMR spectra of (a) PLA, (b) CPPU-20, and (c) CPPU-50 copolymers.

Table 1
Synthesis of 3HB-PLA alternating multiblock copolymer via ROP and chain-extension using HDI.

Samples	Reaction temp. [a] [°C]	Lactide/3HB diol [b] (Theo.) [mol/mol]	Lactide/3HB diol [c] (NMR) [mol/mol]	M_n [d] (GPC) [Da]	M_w [d] (GPC) [Da]	M_w/M_n [d]
BPPU-20	180	20.0	18.5	37,700	106,700	2.83
BPPU-50	180	50.0	50.7	33,800	99,300	2.94
CPPU-20	180	20.0	23.4	27,200	71,100	2.61
CPPU-50	180	50.0	52.7	34,000	78,500	2.31

[a] At 180 °C for 3 h. for ring-opening polymerization and 30 min. for chain extension with HDI.
[b] Theoretical lactide/3HB diol ratio by L-lactide ring-opening polymerization.
[c] Determined by ^{1}H NMR.
[d] Determined by GPC (in DMF).

the shorter PLA segments per repeating unit. These observations support the successful formation of urethane linkages and are consistent with the ^{1}H NMR results. Molecular weights of the copolymers were determined by GPC, with number-average molecular weights (M_n) ranging from approximately 30,000 to 40,000 and dispersity ($Đ = M_w/M_n$) values around 2.5. The M_n values were intentionally kept similar across all samples to ensure that differences in material properties could be attributed to structural variation rather than molecular weight. The data are summarized in Table 1. Together with ^{1}H NMR and FT-IR analyses, these results confirm the successful synthesis of 3HB-PLA alternating multiblock copolymers incorporating different 3HB structures and PLA segment lengths.

The macroscopic appearance of the fabricated films is shown in Fig. S4. Compared to neat PLA, the copolymer films exhibited greater transparency. This observation was supported by UV–Vis transmittance measurements (Fig. S5) and haze analysis (Fig. S6), both of which confirmed the improved optical clarity of the copolymers.

3.2. Thermal properties and crystallinity of 3HB-PLA alternating multiblock copolymers

The thermal properties of the synthesized copolymers were evaluated by DSC, and the results are shown in Fig. 4. The corresponding data are presented in Table 2. Incorporation of 3HB units into the PLA segment led to a decrease in T_g, with a more pronounced reduction observed in copolymers containing shorter PLA segments. BPPU-20 and CPPU-20, which have a higher relative content of 3HB, exhibited no detectable T_m or T_c, indicating that these copolymers are amorphous. This loss of crystallinity and reduction in T_g are attributed to the flexible 3HB segments disrupting the regular packing of PLA segments, which hinders crystallite formation and increases chain mobility [46]. Since PLA's high T_g and semicrystalline nature contribute to its brittleness and slow degradation under ambient conditions, these results suggest that the introduction of 3HB improves flexibility and promote biodegradability [47,48]. T_g values were slightly lower for CPPU compared to BPPU at the same PLA segment length, likely due to the cyclohexane ring in the CPPU backbone introducing additional free volume and reducing intermolecular packing efficiency. For BPPU-50 and CPPU-50, both T_m and T_c peaks were observed, consistent with the presence of crystalline domains associated with longer PLA blocks. Notably, both copolymers exhibited double melting peaks, in contrast to the single T_m of pure PLA. This behavior is commonly attributed to melting-recrystallization-remelting processes or the coexistence of crystallites with different lamellar thicknesses [49].

The XRD patterns of the copolymers are shown in Fig. 5. Neat PLA exhibits sharp diffraction peaks at $2\theta = 16.7°$ and 19.0°, which correspond to the (110)/(200) and (203) planes of the α-crystalline phase, indicating its crystalline nature [50]. CPPU-50 displays peaks at similar positions, though slightly broader and less intense, suggesting the partial

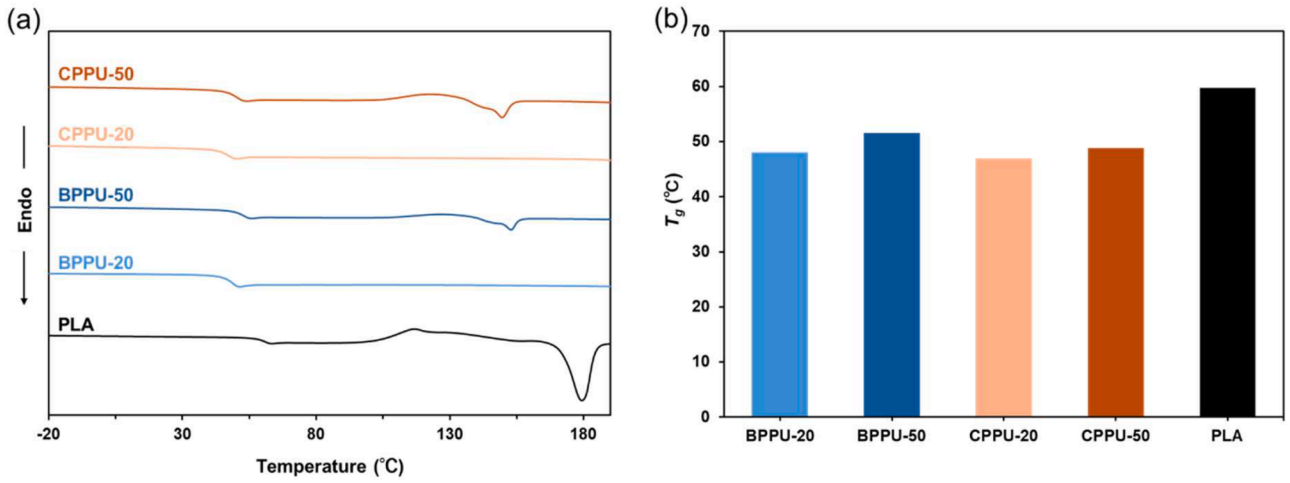

Fig. 4. Thermal properties of PLA and 3HB-PLA alternating multiblock copolymers. (a) Second heating DSC curves; (b) T_g of each sample extracted from the DSC data.

Table 2
Thermal parameters of each sample by DSC. The degree of X_c of each sample determined by XRD.

	Thermal properties (DSC)			XRD
	T_g [°C] [a]	T_c [°C] [a]	T_m [°C] [a]	X_c [%] [b]
BPPU-20	48.0	–[c]	–[c]	20.9
BPPU-50	51.6	127	147, 153	33.8
CPPU-20	46.9	–[c]	–[c]	31.7
CPPU-50	48.8	124	143, 150	48.9
PLA (neat)	59.7	117	179	57.9

[a] Obtained from the second heating scan.
[b] Degree of crystallinity from XRD was calculated.
[c] No thermal transition was detected in the heating process.

retention of crystalline PLA domains after copolymerization with 3HB. In contrast, BPPU-50 exhibits only a broad and weak peak centered near 16°, reflecting a more disordered structure and reduced crystallinity. The crystallinity index values in Table 2, calculated from the XRD patterns using the ratio of crystalline peak area to total area, support this trend. CPPU-50 shows a crystallinity of 48.9 %, while BPPU-50 drops to 33.8 %. The incorporation of 3HB units disrupts the regular packing of PLA segments, leading to a reduction in crystallinity. This effect is more pronounced in copolymers containing linear 3HB, likely due to its greater conformational flexibility compared to cyclic 3HB. As a result, linear 3HB interferes more strongly with PLA segment alignment during crystal formation. Crystallinity decreases further in the CPPU-20 and BPPU-20. CPPU-20 shows only broad, low intensity peaks, while BPPU-20 displays no distinct crystalline peaks, only a broad amorphous halo. This indicates that BPPU-20 is essentially amorphous. Their

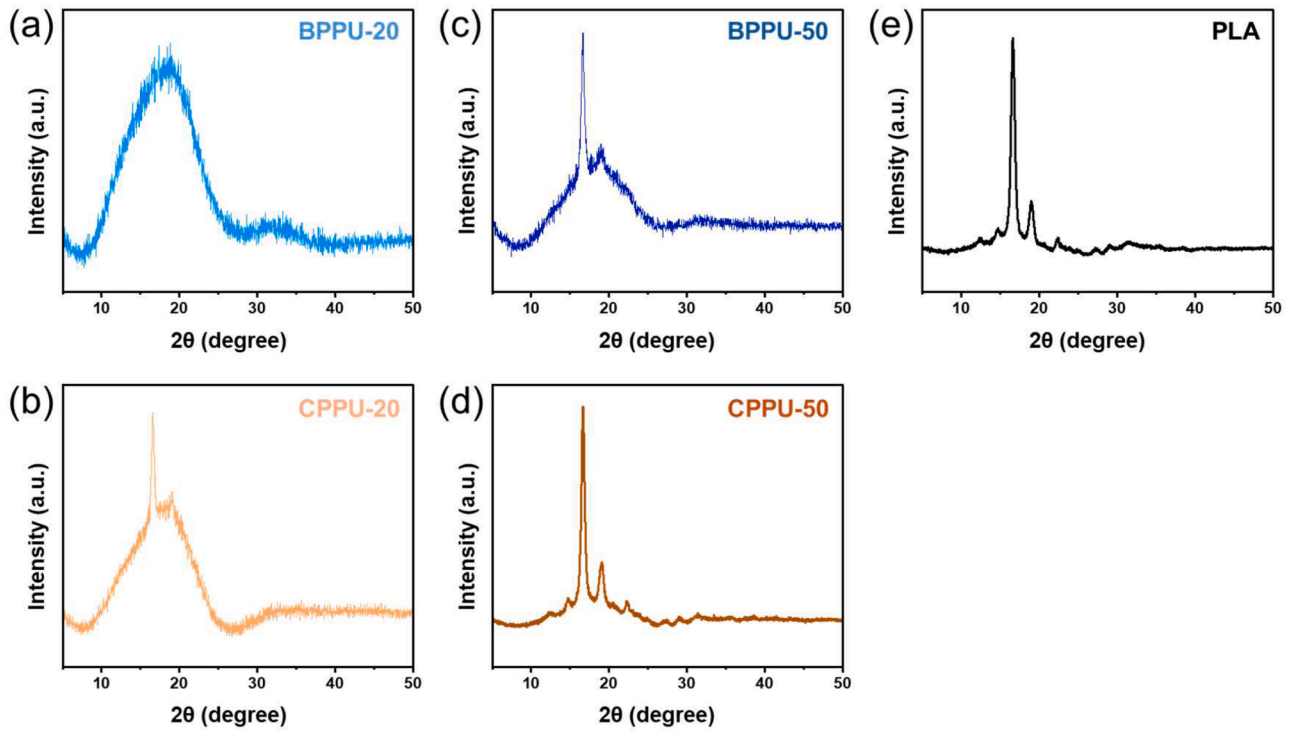

Fig. 5. XRD patterns of (a) BPPU-20, (b) CPPU-20, (c) BPPU-50, (d) CPPU-50, and (e) PLA.

calculated crystallinity values reflect this, with CPPU-20 at 31.7 % and BPPU-20 at 20.9 %. Shorter PLA blocks provide insufficient segment length for effective crystal nucleation and growth, and when combined with the flexibility of linear 3HB, crystallization is almost completely suppressed [51]. Overall, both the incorporation of 3HB and the reduction in PLA block length contribute to the suppression of crystallinity in the copolymers. The structural influence of 3HB units, particularly in their linear form, and the limited crystallizable segment length of PLA blocks act together to increase the amorphous character of the material. These findings are consistent with the thermal behavior observed in DSC, where BPPU-20 and CPPU-20 exhibited no detectable melting or crystallization transitions. Taken together, the structural and thermal results demonstrate that crystallinity can be systematically controlled by adjusting the PLA block length and the 3HB unit structure in the copolymer.

3.3. Thermal stabilities of 3HB-PLA alternating multiblock copolymers

The thermal stability of the 3HB-PLA alternating multiblock copolymers was evaluated by TGA under a nitrogen atmosphere, and the results are presented in Fig. 6. The degradation behavior was assessed based on the temperatures at 15 % and 95 % weight loss ($T_{d,\ 15\ \%}$ and $T_{d,\ 95\ \%}$), which are summarized in Table 3. Compared to neat PLA, all copolymers exhibited lower thermal degradation temperatures. For example, the $T_{d,\ 95\ \%}$ of PLA was 372 °C, whereas the copolymers showed values around 290 °C, indicating a decrease in thermal stability. This decrease can be attributed to the shorter PLA segment lengths in the copolymers and the presence of 3HB units, which are known to degrade at lower temperatures. PHB homopolymers typically exhibit $T_{d,\ 95\ \%}$ values in the range of 250–270 °C, primarily undergoing chain scission through random β-elimination [52,53]. Although the introduction of 3HB reduced the thermal stability relative to PLA, the copolymers still showed improved thermal resistance compared to PHB. This suggests that the presence of PLA blocks stabilizes the copolymer matrix by delaying degradation onset. No clear difference in degradation temperature was observed between copolymers containing cyclic and linear 3HB, suggesting that the nature of the 3HB segment has a minimal influence on bulk thermal decomposition under these conditions. This is because the thermal degradation of polyesters is dominated by random backbone scission at elevated temperatures, which is less sensitive to the stereochemistry or cyclic structure of the repeating units [54].

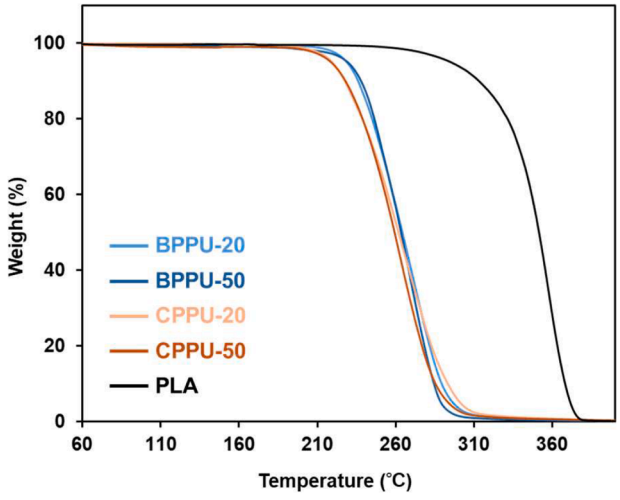

Fig. 6. TGA curves of 3HB-PLA alternating multiblock copolymers and PLA under nitrogen.

Table 3
Thermal parameters of each sample by TGA. Thermal degradation temperatures ($T_{d,\ 15\ \%}$ and $T_{d,\ 95\ \%}$) of PLA and 3HB-PLA alternating multiblock copolymers obtained from TGA under nitrogen.

	Thermal properties (TGA)	
	$T_{d,\ 15\ \%}$ [°C]	$T_{d,\ 95\ \%}$ [°C]
BPPU-20	241	297
BPPU-50	243	289
CPPU-20	233	301
CPPU-50	234	294
PLA (neat)	324	372

3.4. Mechanical properties of 3HB-PLA alternating multiblock copolymers

The mechanical properties of the 3HB-PLA alternating multiblock copolymers were evaluated by tensile testing, and the results are shown in Fig. 7. Fig. 7a presents the stress-strain curves of each sample, while Fig. 7b and Fig. 7c compare the elongation at break and toughness, respectively. A summary of the measured tensile properties, including tensile strength, elongation at break, Young's modulus, and toughness, is provided in Table 4. The incorporation of 3HB units into the PLA backbone led to a significant improvement in elongation at break and toughness, addressing the inherent brittleness of PLA. The extent of improvement depended on both the PLA block length and the 3HB structure. Copolymers with shorter PLA blocks exhibited markedly higher elongation at break, indicating enhanced ductility. In particular, BPPU-20 and CPPU-20 achieved elongation at break values exceeding 400 %, consistent with the low crystallinity and increased segmental mobility observed in DSC and XRD. The influence of 3HB structure was also evident. At equivalent PLA lengths, copolymers containing linear 3HB showed higher elongation at break than those with cyclic 3HB, likely due to the greater chain mobility and conformational flexibility of the linear structure. Among all samples, BPPU-20 exhibited the highest elongation at break, suggesting that the combination of a short PLA block and flexible linear 3HB results in a highly extensible material. BPPU-50 exhibited the highest toughness among the samples, despite its moderate elongation. This likely results from a favorable balance between the crystalline PLA blocks, which provide load-bearing capacity, and the flexible linear 3HB segments, which dissipate energy during deformation. Overall, these results demonstrate that the brittleness of PLA can be effectively addressed through copolymerization with 3HB. The mechanical trends align with the thermal and structural data, confirming that increased amorphous character and chain mobility play a key role in improving the mechanical performance of these materials.

3.5. Enzymatic degradation of 3HB-PLA alternating multiblock copolymers

The enzymatic degradation behavior of 3HB-PLA alternating multiblock copolymer films and neat PLA films was evaluated using proteinase K. As shown in Fig. 8a, mass loss was monitored over time during incubation in Tris-HCl buffer (pH 8.5) containing proteinase K (0.4 mg/mL, 29 units/mg activity) at 20 °C. The degradation rate was calculated from the residual weight of the samples collected at predetermined time points. Compared to neat PLA, all copolymers exhibited higher degradation, indicating improved enzymatic susceptibility. To elucidate the specific role of 3HB units in enzymatic degradation, control multiblock copolymers were synthesized using 1,4-butanediol- and 1,4-cyclohexanedimethanol-initiated PLA oligomers by the same method used for the 3HB-PLA alternating multiblock copolymers (characterized by ^{1}H NMR and GPC; Fig. S7 and Table S1). These 3HB-free copolymers also contain urethane linkages introduced via HDI, allowing for a direct comparison of degradability under structurally similar conditions. As shown in Fig. S8, the 3HB-free copolymers exhibited substantially lower

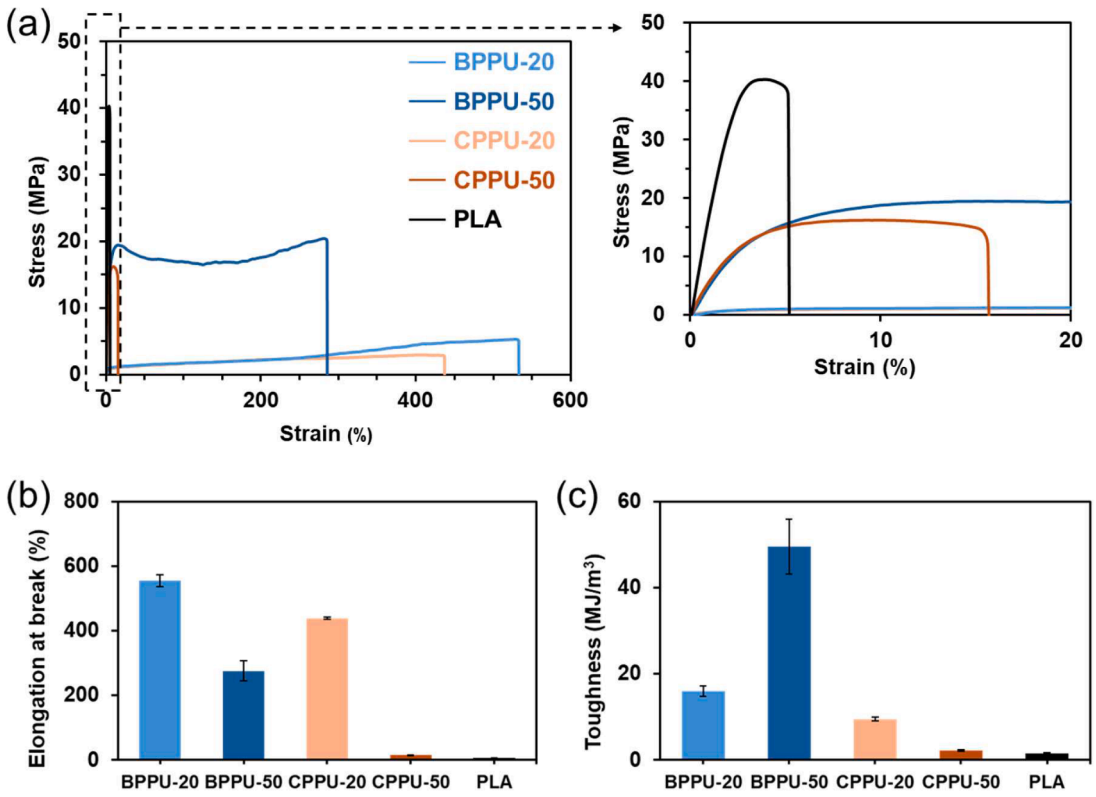

Fig. 7. Tensile properties of 3HB-PLA alternating multiblock copolymers and PLA: (a) stress-strain curves, (b) elongation at break, and (c) toughness.

Table 4
Mechanical properties of each sample by tensile testing.

	Mechanical properties (tensile test)			
	Young's modulus [MPa]	Maximum stress [MPa]	Elongation at break [%]	Toughness [MJ/m]
BPPU-20	30.6 ± 9.9	4.96 ± 0.6	555 ± 19	15.9 ± 1.2
BPPU-50	550 ± 102	20.7 ± 1.5	276 ± 32	49.5 ± 6.4
CPPU-20	59.8 ± 32	3.11 ± 0.3	439 ± 3.2	9.45 ± 0.4
CPPU-50	747 ± 44	16.9 ± 0.6	15.1 ± 0.9	2.19 ± 0.2
PLA (neat)	1740 ± 190	36.0 ±3.8	5.44 ± 0.3	1.54 ± 0.1

enzymatic degradation under identical conditions, indicating that the presence of 3HB units plays a key role in promoting enzymatic susceptibility beyond the influence of urethane linkages alone.

PLA remained largely intact under the test conditions, showing <10 % weight loss after 30 days, reflecting its limited biodegradability under ambient conditions. In contrast, the copolymers degraded more rapidly, particularly those with shorter PLA blocks and higher 3HB content. BPPU-20 and CPPU-20 underwent complete degradation within 10 and 20 days, respectively, reflecting the influence of copolymer architecture on degradation behavior. This enhanced degradability in the copolymers can be attributed to their lower crystallinity and higher amorphous content, as confirmed by DSC and XRD results. Reduced crystalline domains promote greater enzyme accessibility, while the flexible 3HB segments increase chain mobility, facilitating interactions between enzyme and substrate [55]. Notably, copolymers with linear 3HB (BPPU) showed faster degradation than their cyclic counterparts (CPPU) at equivalent PLA lengths. Linear architecture is likely to provide higher conformational flexibility and less steric hindrance, allowing a more efficient enzymatic attack.

Fig. 8c and 8d present the macroscopic and microscopic changes in film morphology before and after degradation (Fig. S9-13). For each sample, the post-degradation images correspond to the time point showing the most pronounced degradation before complete film disintegration. Since degradation rates varied across samples, the time points differed accordingly. As biodegradation progressed, all copolymer films showed a gradual loss of transparency. The rate of increase in opacity closely followed the degradation trend, with BPPU-20 transitioning to an opaque state most rapidly. In contrast, PLA films showed minimal visual change, consistent with their low degradation. The loss of transparency is attributed to surface roughening, microcrack formation, and light scattering caused by increased structural disorder, all of which were confirmed by SEM. Additionally, surface morphology resembling spherulites was observed after enzymatic degradation in most copolymer films. These features were particularly prominent in BPPU-20 and CPPU-20, suggesting the presence of spherulitic structures and the preferential enzymatic degradation of amorphous domains [56, 57].

To further examine the relationship between surface properties and enzymatic degradation, WCA measurements were conducted (Fig. 8b). Neat PLA exhibited a relatively high contact angle of 88.4°, indicating a hydrophobic surface. In contrast, all copolymers showed lower contact angles, with BPPU samples displaying lower values than CPPU. BPPU-20 exhibited the greatest surface wettability, with a contact angle of 77°, suggesting improved hydrophilicity. This change is likely influenced by structural differences introduced through the incorporation of 3HB units and the associated increase in urethane linkages in copolymers with

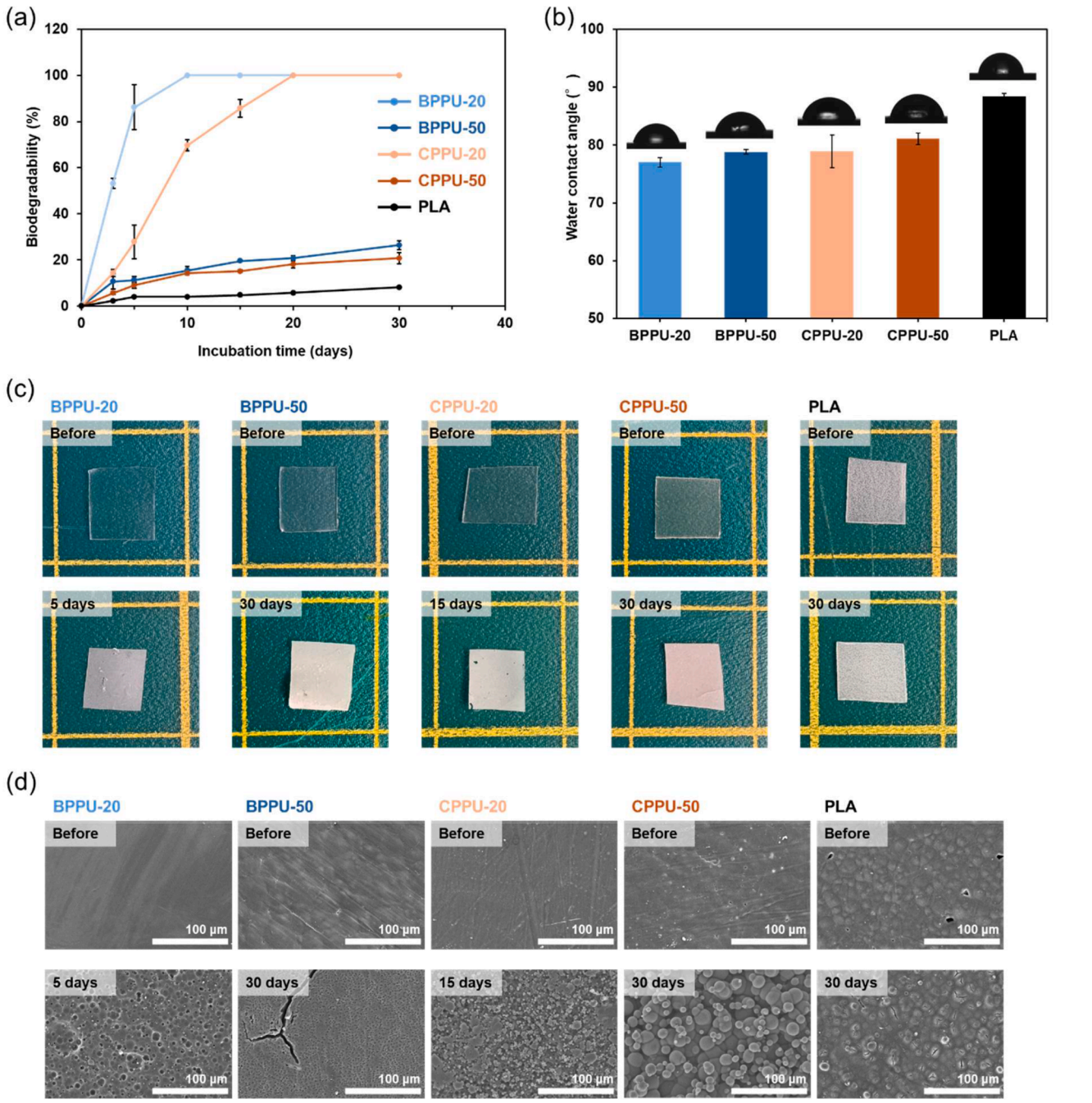

Fig. 8. Enzymatic degradation behavior and surface properties of 3HB-PLA alternating multiblock copolymer films and neat PLA: (a) mass loss profiles over time during enzymatic degradation, (b) WCA measurements before degradation, (c) macroscopic changes in film appearance at representative degradation time points, and (d) microscopic surface morphology observed by SEM after degradation.

shorter PLA segments. Although the individual contributions of these factors cannot be clearly separated, both are expected to influence surface polarity. This trend correlates well with the degradation data, as higher surface wettability is expected to facilitate water penetration and enzyme diffusion, enhancing hydrolysis at the film surface [58].

To gain deeper insight into the degradation mechanism, ^{1}H NMR was conducted, and the results are presented in Fig. S14-S16. In the 3HB-PLA alternating multiblock copolymers, a progressive decrease in the methyl resonance of the lactic acid repeat units (1.55–1.57 ppm), accompanied by a corresponding increase in a shoulder signal attributed to PLA oligomers (~1.53 ppm), was observed. These spectral changes indicate progressive main-chain scission and the accumulation of low-molecular-weight degradation products. In contrast, the ^{1}H NMR spectra of neat PLA showed minimal changes, consistent with its limited enzymatic degradation.

Collectively, the enzymatic degradation of 3HB-PLA alternating multiblock copolymers is governed by the combined effects of chain mobility, crystallinity, and surface hydrophilicity. BPPU-20 exhibited the highest degradation rate, which can be attributed to its linear 3HB segments, short PLA block length, and low crystallinity. These structural features enhance enzymatic accessibility by reducing steric hindrance and increasing segmental motion in the amorphous regions. In contrast, copolymers with longer PLA blocks showed slower degradation due to reduced accessibility and the need for multiple chain scission events within more ordered domains. These findings demonstrate that both the incorporation of 3HB units and the modulation of PLA segment length

are key parameters in controlling degradability. The ability to tune degradation behavior through molecular design provides a promising strategy for developing environmentally responsive and biodegradable polymeric materials.

4. Conclusion

To overcome the intrinsic brittleness and limited biodegradability of PLA under ambient conditions, a series of 3HB-PLA alternating multiblock copolymers were synthesized via copolymerization with either linear or cyclic 3HB diols. The incorporation of 3HB was intended to enhance segmental flexibility while leveraging the known environmental degradability of 3HB-based polyesters, particularly in natural settings such as marine environments. Systematic variation of both 3HB architecture and PLA block length enabled a comprehensive evaluation of how molecular structure governs the thermal, mechanical, and degradative behavior of these materials. XRD and DSC analyses revealed that 3HB disrupts the crystalline domains of PLA, particularly in copolymers containing short PLA segments and linear 3HB units. This disruption led to increased film transparency and reduced T_g, indicating enhanced chain mobility and greater potential for ductile behavior. These structural and thermal modifications translated into improved mechanical performance, with BPPU-20 exhibiting the highest elongation at break and BPPU-50 achieving the greatest toughness among the copolymers examined. Enzymatic degradation studies demonstrated significantly accelerated degradation in all copolymers compared to neat PLA, with the rate strongly influenced by crystallinity, segmental dynamics, and surface hydrophilicity. BPPU-20, characterized by short PLA blocks and flexible linear 3HB segments, degraded completely within 10 days. SEM and contact angle analyses supported these findings, revealing substantial surface erosion and increased hydrophilicity. These insights offer a rational framework for designing degradable multiblock systems with controlled breakdown behavior.

This study demonstrates that alternating 3HB-PLA multiblock copolymers offer a versatile platform for tailoring both the mechanical and biodegradation profiles of PLA-based materials. By fine-tuning block architecture, it is possible to systematically address key limitations of PLA, paving the way for its expanded use in environmentally responsive applications such as compostable packaging, agricultural films, and biomedical devices. These findings contribute to the broader development of sustainable polymer systems that balance performance with end-of-life degradability.

CRediT authorship contribution statement

Konosuke Yoshida: Writing – original draft, Validation, Methodology, Investigation, Data curation, Conceptualization. **Yu-I Hsu:** Writing – review & editing, Visualization, Methodology, Funding acquisition, Conceptualization. **Masayuki Sugimoto:** Resources, Methodology, Conceptualization. **Hiroshi Uyama:** Supervision, Project administration, Funding acquisition.

Declaration of competing interest

The authors declare that they have no known competing financial interests or personal relationships that could have appeared to influence the work reported in this paper.

Acknowledgements

This work was supported by Japan Science and Technology Agency (JST) PRESTO Grant Number JPMJPR23N4, the Environment Research and Technology Development Fund JPMEERF21S11900 of the Environmental Restoration and Conservation Agency of Japan, and Japan Society for the Promotion of Science (JSPS) KAKENHI Grants (22K21348 and 23K26717). We gratefully acknowledge Osaka Gas for providing (*R*)-3-hydroxybutyric acid (3HB) and for their cooperation in advancing this research. The first author gratefully acknowledges scholarship support from the Tobe Maki Scholarship Foundation.

Supplementary materials

Supplementary material associated with this article can be found, in the online version, at doi:10.1016/j.polymdegradstab.2025.111570.

Data availability

No data was used for the research described in the article.

References

[1] S. Zhao, L. Zhu, Plastic carbon in the ocean, Curr. Opin. Chem. Eng. (2025) 101101, https://doi.org/10.1016/j.coche.2025.101101.
[2] J.R. Jambeck, R. Geyer, C. Wilcox, T.R. Siegler, M. Perryman, A. Andrady, R. Narayan, K.L. Law, Plastic waste inputs from land into the ocean, Science 347 (2015) 768–771, https://doi.org/10.1126/science.1260352.
[3] A. Chamas, H. Moon, J. Zheng, Y. Qiu, T. Tabassum, J.H. Jang, M. Abu-Omar, S. L. Scott, S. Suh, Degradation rates of plastics in the environment, ACS Sustain. Chem. Eng. 8 (2020) 3494–3511, https://doi.org/10.1021/acssuschemeng.9b06635.
[4] M.A. Fayshal, Current practices of plastic waste management, environmental impacts, and potential alternatives for reducing pollution and improving management, Heliyon 10 (2024) e40838, https://doi.org/10.1016/j.heliyon.2024.e40838.
[5] S.S. Ali, M.H.M. Alsharbaty, R. Al-Tohamy, M. Schagerl, M. Al-Zahrani, M. Kornaros, J. Sun, Microplastics as persistent and vectors of other threats in the marine environment: toxicological impacts, management and strategical roadmap to end plastic pollution, Environ. Chem. Ecotoxicol. 7 (2025) 229–251, https://doi.org/10.1016/j.enceco.2024.12.005.
[6] G. Atiwesh, A. Mikhael, C.C. Parrish, J. Banoub, T.-A.T. Le, Environmental impact of bioplastic use: a review, Heliyon 7 (2021) e07918, https://doi.org/10.1016/j.heliyon.2021.e07918.
[7] L. Manfra, V. Marengo, G. Libralato, M. Costantini, F. De Falco, M. Cocca, Biodegradable polymers: a real opportunity to solve marine plastic pollution? J. Hazard. Mater. 416 (2021) 125763 https://doi.org/10.1016/j.jhazmat.2021.125763.
[8] V. Suresh, R. Shams, K.K. Dash, A.M. Shaikh, K. Béla, Comprehensive review on enzymatic polymer degradation: a sustainable solution for plastics, J. Agric. Food Res. 20 (2025) 101788, https://doi.org/10.1016/j.jafr.2025.101788.
[9] A.S. Barone, C. Maragoni-Santos, P.M. de Farias, C.M.G. Cortat, B.C. Maniglia, R. S. Ongaratto, S. Ferreira, A.E.C. Fai, Rethinking single-use plastics: innovations, polices, consumer awareness and market shaping biodegradable solutions in the packaging industry, Trends Food Sci. Technol. 158 (2025) 104906, https://doi.org/10.1016/j.tifs.2025.104906.
[10] V. Beghetto, V. Gatto, R. Samiolo, C. Scolaro, S. Brahimi, M. Facchin, A. Visco, Plastics today: key challenges and EU strategies towards carbon neutrality: a review, Environ. Pollut. 334 (2023) 122102, https://doi.org/10.1016/j.envpol.2023.122102.
[11] O. Buchholz, Recent progress on the promotion and standardization of bioplastics in Japan, Eur. Bioplastics EV (2022). https://www.european-bioplastics.org/recent-progress-on-the-promotion-and-standardization-of-bioplastics-in-japan/ (accessed April 21, 2025).
[12] S. Farah, D.G. Anderson, R. Langer, Physical and mechanical properties of PLA, and their functions in widespread applications — A comprehensive review, Adv. Drug Deliv. Rev. 107 (2016) 367–392, https://doi.org/10.1016/j.addr.2016.06.012.
[13] R.M. Rasal, D.E. Hirt, Toughness decrease of PLA-PHBHHx blend films upon surface-confined photopolymerization, J. Biomed. Mater. Res. A 88A (2009) 1079–1086, https://doi.org/10.1002/jbm.a.32009.
[14] R.M. Rasal, A.V. Janorkar, D.E. Hirt, Poly(lactic acid) modifications, Prog. Polym. Sci. 35 (2010) 338–356, https://doi.org/10.1016/j.progpolymsci.2009.12.003.
[15] H. Liu, J. Zhang, Research progress in toughening modification of poly(lactic acid), J. Polym. Sci. Part B Polym. Phys. 49 (2011) 1051–1083, https://doi.org/10.1002/polb.22283.
[16] Y.-P. Song, D.-Y. Wang, X.-L. Wang, L. Lin, Y.-Z. Wang, A method for simultaneously improving the flame retardancy and toughness of PLA, Polym. Adv. Technol. 22 (2011) 2295–2301, https://doi.org/10.1002/pat.1760.
[17] T. Qiang, D. Yu, H. Gao, Wood flour/polylactide biocomposites toughened with polyhydroxyalkanoates, J. Appl. Polym. Sci. 124 (2012) 1831–1839, https://doi.org/10.1002/app.35224.
[18] T.P. Haider, C. Völker, J. Kramm, K. Landfester, F.R. Wurm, Plastics of the future? The impact of biodegradable polymers on the environment and on society, Angew. Chem. Int. Ed. 58 (2019) 50–62, https://doi.org/10.1002/anie.201805766.
[19] J.H. Song, R.J. Murphy, R. Narayan, G.B.H. Davies, Biodegradable and compostable alternatives to conventional plastics, Philos. Trans. R. Soc. B Biol. Sci. 364 (2009) 2127–2139, https://doi.org/10.1098/rstb.2008.0289.
[20] S.-J. Royer, F. Greco, M. Kogler, D.D. Deheyn, Not so biodegradable: polylactic acid and cellulose/plastic blend textiles lack fast biodegradation in marine waters, PLOS One 18 (2023) e0284681, https://doi.org/10.1371/journal.pone.0284681.

[21] S. Phosri, T. Kunjiek, C. Mukkhakang, S. Suebthep, W. Sinsup, S. Phornsirigarn, P. Charoeythornkhajhornchai, Biodegradability of bioplastic blown film in a marine environment, Front. Mar. Sci. 9 (2022), https://doi.org/10.3389/fmars.2022.917397.
[22] L. Wang, W. Ma, R.A. Gross, S.P. McCarthy, Reactive compatibilization of biodegradable blends of poly(lactic acid) and poly(ε-caprolactone), Polym. Degrad. Stab. 59 (1998) 161–168, https://doi.org/10.1016/S0141-3910(97)00196-1.
[23] C.-C. Chen, J.-Y. Chueh, H. Tseng, H.-M. Huang, S.-Y. Lee, Preparation and characterization of biodegradable PLA polymeric blends, Biomaterials 24 (2003) 1167–1173, https://doi.org/10.1016/S0142-9612(02)00466-0.
[24] O. Prasitnok, K. Prasitnok, Architectural effects of biodegradable block copolymers on enhancing PLA/PCL blend compatibility: molecular dynamics simulations, Macromolecules (2025), https://doi.org/10.1021/acs.macromol.5c00158.
[25] C. Zhang, T. Zhai, L.-S. Turng, Y. Dan, Morphological, mechanical, and crystallization behavior of polylactide/polycaprolactone blends compatibilized by l-lactide/caprolactone copolymer, Ind. Eng. Chem. Res. 54 (2015) 9505–9511, https://doi.org/10.1021/acs.iecr.5b02134.
[26] W. Wen, C. Li, X. Meng, W. Gong, S. Chen, Z. Xin, Study on compatibility of a novel cardanol-based compatibilizer in PLA/PBAT blend, Ind. Eng. Chem. Res. 63 (2024) 8684–8696, https://doi.org/10.1021/acs.iecr.4c00634.
[27] D. Wu, Y. Zhang, L. Yuan, M. Zhang, W. Zhou, Viscoelastic interfacial properties of compatibilized poly(ε-caprolactone)/polylactide blend, J. Polym. Sci. Part B Polym. Phys. 48 (2010) 756–765, https://doi.org/10.1002/polb.21952.
[28] Y. Ding, W. Feng, B. Lu, P. Wang, G. Wang, J. Ji, PLA-PEG-PLA tri-block copolymers: effective compatibilizers for promotion of the interfacial structure and mechanical properties of PLA/PBAT blends, Polymer 146 (2018) 179–187, https://doi.org/10.1016/j.polymer.2018.05.037.
[29] K. Formela, L. Zedler, A. Hejna, A. Tercjak, Reactive extrusion of bio-based polymer blends and composites – current trends and future developments, Express Polym. Lett. 12 (2018) 24–57, https://doi.org/10.3144/expresspolymlett.2018.4.
[30] I. Plamadiala, C. Croitoru, M.A. Pop, I.C. Roata, Enhancing polylactic acid (PLA) performance: a review of additives in fused deposition modelling (FDM) filaments, Polymers 17 (2025) 191, https://doi.org/10.3390/polym17020191.
[31] K. Wang, Y. Chen, H. Long, M. Baghani, Y. Rao, Y. Peng, Hygrothermal aging effects on the mechanical properties of 3D printed composites with different stacking sequence of continuous glass fiber layers, Polym. Test. 100 (2021) 107242, https://doi.org/10.1016/j.polymertesting.2021.107242.
[32] S. Thumsorn, W. Prasong, T. Kurose, A. Ishigami, Y. Kobayashi, H. Ito, Rheological behavior and dynamic mechanical properties for interpretation of layer adhesion in FDM 3D printing, Polymers 14 (2022) 2721, https://doi.org/10.3390/polym14132721.
[33] X. Cui, A. Ozaki, T.-A. Asoh, H. Uyama, Cellulose modified by citric acid reinforced poly(lactic acid) resin as fillers, Polym. Degrad. Stab. 175 (2020) 109118, https://doi.org/10.1016/j.polymdegradstab.2020.109118.
[34] A. Takagi, Y.-I. Hsu, H. Uyama, Biodegradable poly(lactic acid) and polycaprolactone alternating multiblock copolymers with controllable mechanical properties, Polym. Degrad. Stab. 218 (2023) 110564, https://doi.org/10.1016/j.polymdegradstab.2023.110564.
[35] M. He, Y.-I. Hsu, H. Uyama, Superior sequence-controlled poly(L-lactide)-based bioplastic with tunable seawater biodegradation, J. Hazard. Mater. 474 (2024) 134819, https://doi.org/10.1016/j.jhazmat.2024.134819.
[36] F.B. Ali, D.J. Kang, M.P. Kim, C.-H. Cho, B.J. Kim, Synthesis of biodegradable and flexible, polylactic acid based, thermoplastic polyurethane with high gas barrier properties, Polym. Int. 63 (2014) 1620–1626, https://doi.org/10.1002/pi.4662.
[37] M. Suzuki, Y. Tachibana, K. Kasuya, Biodegradability of poly(3-hydroxyalkanoate) and poly(ε-caprolactone) via biological carbon cycles in marine environments, Polym. J. 53 (2021) 47–66, https://doi.org/10.1038/s41428-020-00396-5.
[38] D. Garcia-Garcia, L. Quiles-Carrillo, R. Balart, S. Torres-Giner, M.P. Arrieta, Innovative solutions and challenges to increase the use of Poly(3-hydroxybutyrate) in food packaging and disposables, Eur. Polym. J. 178 (2022) 111505, https://doi.org/10.1016/j.eurpolymj.2022.111505.
[39] H.J. Tang, S.Z. Neoh, K. Sudesh, A review on poly(3-hydroxybutyrate-co-3-hydroxyhexanoate) [P(3HB-co-3HHx)] and genetic modifications that affect its production, Front. Bioeng. Biotechnol. 10 (2022), https://doi.org/10.3389/fbioe.2022.1057067.
[40] M. Jo, Y. Jang, E. Lee, S. Shin, H.-J. Kang, The modification of poly(3-Hydroxybutyrate-co-4-hydroxybutyrate) by melt blending, Polymers 14 (2022) 1725, https://doi.org/10.3390/polym14091725.
[41] H. Abe, Y. Doi, Y. Hori, T. Hagiwara, Physical properties and enzymatic degradability of copolymers of (*R*)-3-hydroxybutyric acid and (*S,S*)-lactide, Polymer 39 (1998) 59–67, https://doi.org/10.1016/S0032-3861(97)00240-1.
[42] M. Yamada, K. Matsumoto, T. Nakai, S. Taguchi, Microbial production of lactate-enriched poly[(R)-lactate-co-(R)-3-hydroxybutyrate] with novel thermal properties, Biomacromolecules 10 (2009) 677–681, https://doi.org/10.1021/bm8013846.
[43] S. Hiki, M. Miyamoto, Y. Kimura, Synthesis and characterization of hydroxy-terminated [RS]-poly(3-hydroxybutyrate) and its utilization to block copolymerization with l-lactide to obtain a biodegradable thermoplastic elastomer, Polymer 41 (2000) 7369–7379, https://doi.org/10.1016/S0032-3861(00)00086-0.
[44] L. Wu, S. Chen, Z. Li, K. Xu, G.-Q. Chen, Synthesis, characterization and biocompatibility of novel biodegradable poly[((R)-3-hydroxybutyrate)-block-(D,L-lactide)-block-(ε-caprolactone)] triblock copolymers, Polym. Int. 57 (2008) 939–949, https://doi.org/10.1002/pi.2431.
[45] Y. Tabata, H. Abe, Effects of composition and sequential structure on thermal properties for copolymer of 3-hydroxybutyrate and lactate units, Polym. Degrad. Stab. 98 (2013) 1796–1803, https://doi.org/10.1016/j.polymdegradstab.2013.05.014.
[46] S. Saeidlou, M.A. Huneault, H. Li, C.B. Park, Poly(lactic acid) crystallization, Prog. Polym. Sci. 37 (2012) 1657–1677, https://doi.org/10.1016/j.progpolymsci.2012.07.005.
[47] O. Okolie, A. Kumar, C. Edwards, L.A. Lawton, A. Oke, S. McDonald, V.K. Thakur, J. Njuguna, Bio-based sustainable polymers and materials: from processing to biodegradation, J. Compos. Sci. 7 (2023) 213, https://doi.org/10.3390/jcs7060213.
[48] P.M.S. Souza, A.R. Morales, M.A. Marin-Morales, L.H.I. Mei, PLA and montmorilonite nanocomposites: properties, biodegradation and potential toxicity, J. Polym. Environ. 21 (2013) 738–759, https://doi.org/10.1007/s10924-013-0577-z.
[49] L.M.W.K. Gunaratne, R.a. Shanks, Miscibility, melting, and crystallization behavior of poly(hydroxybutyrate) and poly(D,L-lactic acid) blends, Polym. Eng. Sci. 48 (2008) 1683–1692, https://doi.org/10.1002/pen.21051.
[50] S.H. Tabatabaei, A. Ajji, Crystal structure and orientation of uniaxially and biaxially oriented PLA and PP nanoclay composite films, J. Appl. Polym. Sci. 124 (2012) 4854–4863, https://doi.org/10.1002/app.35563.
[51] Z. Refaa, M. Boutaous, D.A. Siginer, PLA crystallization kinetics and morphology development, Int. Polym. Process. 33 (2018) 336–344, https://doi.org/10.3139/217.3525.
[52] M. Kervran, C. Vagner, M. Cochez, M. Ponçot, M.R. Saeb, H. Vahabi, Thermal degradation of polylactic acid (PLA)/polyhydroxybutyrate (PHB) blends: a systematic review, Polym. Degrad. Stab. 201 (2022) 109995, https://doi.org/10.1016/j.polymdegradstab.2022.109995.
[53] M.Y. Lee, T.S. Lee, W.H. Park, Effect of side chains on the thermal degradation of poly(3-hydroxyalkanoates), Macromol. Chem. Phys. 202 (2001) 1257–1261, https://doi.org/10.1002/1521-3935(20010401)202:7<1257::AID-MACP1257>3.0.CO;2-Y.
[54] A. Gleadall, J. Pan, M.-A. Kruft, M. Kellomäki, Degradation mechanisms of bioresorbable polyesters. Part 1. Effects of random scission, end scission and autocatalysis, Acta Biomater. 10 (2014) 2223–2232, https://doi.org/10.1016/j.actbio.2013.12.039.
[55] S. Li, S. McCarthy, Influence of crystallinity and stereochemistry on the enzymatic degradation of poly(lactide)s, Macromolecules 32 (1999) 4454–4456, https://doi.org/10.1021/ma990117b.
[56] N. Kimura, T. Kabe, S. Kimura, K. Kasuya, T. Iwata, Enzymatic degradation mechanism of the lamellar stacking structures of poly([*R*]-3-hydroxybutyrate-*co*-[*R*]-3-hydroxyvalerate) fibers, Polym. Degrad. Stab. 219 (2024) 110607, https://doi.org/10.1016/j.polymdegradstab.2023.110607.
[57] Y. Kikkawa, H. Abe, T. Iwata, Y. Inoue, Y. Doi, Crystallization, stability, and enzymatic degradation of poly(l-lactide) thin film, Biomacromolecules 3 (2002) 350–356, https://doi.org/10.1021/bm015623z.
[58] H. Tsuji, T. Ishida, N. Fukuda, Surface hydrophilicity and enzymatic hydrolyzability of biodegradable polyesters: 1. effects of alkaline treatment, Polym. Int. 52 (2003) 843–852, https://doi.org/10.1002/pi.1199.